Geochemical Perspectives Letters

On the stability of acetate in subduction zone fluids

V. Szlachta[1], K. Vlasov[1], H. Keppler[1*]

https://doi.org/10.7185/geochemlet.2213

Abstract

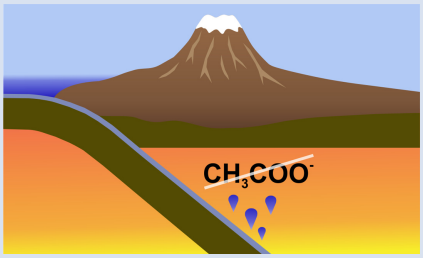

Recent theoretical studies have suggested that, under certain intermediate redox conditions, organic anions, in particular acetate, may be the dominant carbon species in deep subduction zone fluids. This could have major consequences for the properties of these fluids, for the formation of diamonds, and for the deep carbon cycle in general. We have tested these predictions by carrying out both *ex situ* piston cylinder experiments and *in situ* Raman spectroscopic experiments in the externally heated diamond cell, with a temperature up to 600 °C and pressure up to 5 GPa, the predicted stability field of acetate. We observed that upon heating and pressurisation to these conditions, an aqueous solution of sodium acetate undergoes several interesting reactions, including the formation of higher hydrocarbons. However, at 5 GPa and 600 °C, almost all organic species appear to have decomposed to a graphite-like material. Our experiments, therefore, do not support the stability of acetate and other organics as main carbon species in deep subduction fluids. However, the stability of minor concentrations of such species is still possible and requires further study. During deep subduction, most of the reduced carbon in sediments may be retained and recycled into the mantle to great depth.

Received 9 December 2021 | Accepted 1 April 2022 | Published 22 April 2022

Introduction

Aqueous fluids released from the subducted slab are likely the main agent for melting and mass transport in subduction zones (*e.g.*, Tatsumi, 1989; Manning and Frezzotti, 2020; Rustioni *et al.*, 2021). They also return subducted volatiles, such as water, carbon, and nitrogen back to the surface. Over long geologic time, this fluid flux, therefore, is involved in the processes regulating global sea level (*e.g.*, Rüpke *et al.*, 2004), the carbon dioxide content of the atmosphere (*e.g.*, Plank and Manning 2019), and climate. Traditionally, the fluids released by the dehydration of hydrous minerals, such as amphibole and serpentine, were considered to consist of simple solvent molecules, *i.e.* mostly H_2O and CO_2, plus some dissolved inorganic species (*e.g.*, Manning, 2004). However, recently theoretical predictions have emerged which suggest that, in high pressure subduction fluids, most of the carbon may under some redox and pH conditions be present as organic molecules, such as acetate (Sverjensky *et al.*, 2014, 2020; Sverjensky and Huang, 2015). In particular, acetate was predicted to be the predominant carbon species in aqueous fluids at 5 GPa, 600 °C, and intermediate redox conditions ($\log f O_2 = 10^{-16}$ to 10^{-19} bar, one to four log units below the QFM = quartz fayalite magnetite buffer). Organic species in aqueous high pressure fluids have also been invoked to explain elevated solubilities of the forsterite + enstatite and magnesite + enstatite assemblages in the presence of carbon (Tiraboschi *et al.*, 2018). Similarly, Tumiati *et al.* (2017) attributed the increase of CO_2 molar fraction in COH fluids upon in the presence of silica to the formation of some organic complexes involving Si.

Evidence for the stability of acetate and similar organic species either from observations in natural samples or from high pressure experiments is up to now rather limited. Frezzotti (2019) studied fluid inclusions in diamond-bearing rocks from the Alps by Raman spectroscopy. She concluded that the data provide evidence that diamond surfaces are coated by sp^2- and sp^3-bonded amorphous carbon containing functional groups of carboxylic acids. This conclusion is, however, based on the deconvolution of rather broad Raman bands into various components and on band assignments that may not be unique. Huang *et al.* (2017) heated sodium acetate solutions in an externally heated diamond cell to 300 °C and 2.4–3.5 GPa and observed the partial decomposition of acetate to immiscible isobutane. However, they did not reach the predicted *P-T* stability field of acetate and it remains unclear whether the isobutane observed in these experiments is a stable species or just an intermediate, metastable decomposition product of the acetate. Li (2016) studied the speciation in aqueous C–H–O fluids using synthetic fluid inclusions. He observed traces of ethane and perhaps higher hydrocarbons together with methane at 2.5 GPa, 600 °C, and Fe–FeO buffer conditions, but no indication of acetate or other organic acid anions. We, therefore, carried out some exploratory experiments to test the predicted stability of acetate at 5 GPa and 600 °C.

Methods

All experiments were carried out with a solution of 10 wt. % of sodium acetate ($CH_3COONa \cdot 3\ H_2O$) in water. We made no attempt to externally buffer oxygen fugacity or pH. Rather, we assumed that if acetate were stable, it should, at high

1. Bayerisches Geoinstitut, Universität Bayreuth, 95440 Bayreuth, Germany
* Corresponding author (email: Hans.Keppler@uni-bayreuth.de)

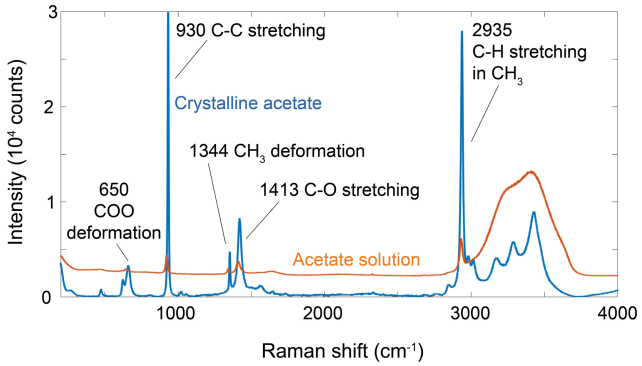

Figure 1 Raman spectra of crystalline sodium acetate ($CH_3COONa \cdot 3\ H_2O$) and of a 10 wt. % solution of sodium acetate in water, measured at ambient conditions.

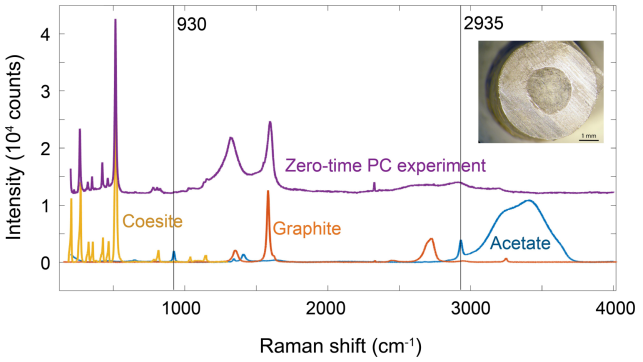

Figure 2 Raman spectrum of run products from a "zero-time" piston cylinder experiment (purple) at 5 GPa and 600 °C. Reference spectra of the initial acetate solution (blue), of graphite (orange) and of coesite (yellow) are shown for comparison. Neither the 930 cm^{-1} nor the 2935 cm^{-1} band of acetate can be detected in the run products. The inset shows the opened silver capsule with the charge. The grey discoloration is due to a carbonaceous material formed by decomposition of acetate.

concentrations, buffer these parameters to its intrinsic stability range. We carried out two types of experiments:

(1) Piston cylinder experiments using very thick-walled silver capsules. Silver is poorly permeable for hydrogen at 600 °C (Chou, 1986), such that hydrogen loss from the capsule should be minimal and the intrinsic oxygen fugacity of the solution should be preserved during the experiments. Runs were designed to form a times series, from a nominally "zero-time experiment" (quenching 8 minutes after heating to 600 °C at 5 GPa) to 24 hours run duration. For mechanical stabilisation, capsules were filled with silica powder in addition to the acetate solution. The use of silica is realistic for subduction zone fluids, as even MORB eclogites usually contain a trace of free quartz or coesite (Sisson and Kelemen, 2018). Run products were investigated by Raman spectroscopy and by powder-ray diffraction.

(2) *In situ* experiments using externally heated diamond anvil cells. Here, the solution was directly observed under a microscope and studied by Raman spectroscopy during different heating and cooling paths. In one of these experiments, we reached 4.65 GPa and 600 °C, essentially the predicted stability field of acetate.

Since Raman spectroscopy was used as the main tool for identifying acetate and other organic species, Figure 1 shows the Raman spectra of both crystallised sodium acetate and of the 10 wt. % sodium acetate solution used in our experiments. Band assignments are after Ito and Bernstein (1956). For identifying acetate in the experiments, we mostly relied on the strong C–C stretching band near 930 cm^{-1} and the C–H stretching vibration of the methyl group at 2935 cm^{-1}.

Further details on the experimental methods are given in the Supplementary Information.

Results from Piston Cylinder Experiments

The piston cylinder experiments were all carried out at 5 GPa and 600 °C, with run durations of 0.1, 0.5, 2, 6, and 24 hours. In all runs, the SiO_2 powder had been converted to coesite, as indicated by X-ray diffraction. No other crystalline phases were detected. Raman spectra of the quenched run products (Fig. 2) failed to detect any acetate. Instead, bands similar to a highly disordered graphite or perhaps kerogen-like material were observed. This is consistent with the grey discoloration observed in the run products (Fig. 2). There was no fundamental difference between the results of the "zero-time" experiment and the experiments with longer run durations up to 24 hours; only the bands of the carbonaceous material became narrower with increasing run duration.

Results from *in situ* Experiments in the Diamond Cell

A total of four experiments were carried out by heating the acetate solution in the diamond anvil cell. Detailed pressure-temperature paths for all experiments are given in the Supplementary Figures S-1 and S-2. Run AB1 reached a maximum of 125 °C and 2.25 GPa before losing pressure. The Raman spectrum of acetate was observed up to the maximum temperature; the solution remained clear and no decomposition products of acetate were detectable. After cooling to room temperature, pressure was increased by tightening the cell such that the solution solidified to ice. Run AB2 was then conducted with this charge and reached 350 °C and 2.93 GPa before the gasket cracked. In this experiment, some dark precipitate started to form around 150 °C. However, as shown in Figure 3a, even at the highest temperatures, the C–C stretching bands (930 cm^{-1}) and the C–H stretching bands (2935 cm^{-1}) of acetate were still detectable in the Raman spectrum of the solution, although shifted to slightly higher wave numbers due to the elevated pressure. After cooling experiment AB2 to room temperature, bubbles of an immiscible liquid were observed inside the sample chamber. Raman spectra (Fig. 3b) suggest that they consist of newly formed hydrocarbons, in particular propane and isobutane, in very good agreement with similar observations made by Huang *et al.* (2017). The formation of propane and isobutane suggests that, already under these rather mild conditions, new C–C bonds may form rapidly, probably via some radical mechanism. In particular, the reaction of acetate to isobutane requires a complete rearrangement of the C–C bonds.

Experiment AB3 reached maximum conditions of 400 °C and 3.50 GPa. After cooling to room temperature, some patches of dark material were visible in the solution and a small crystal of an alkali carbonate (not further identified) was detected by Raman spectroscopy, similar to observations made by Huang *et al.* (2017). The carbonate (with C^{4+}) likely formed together

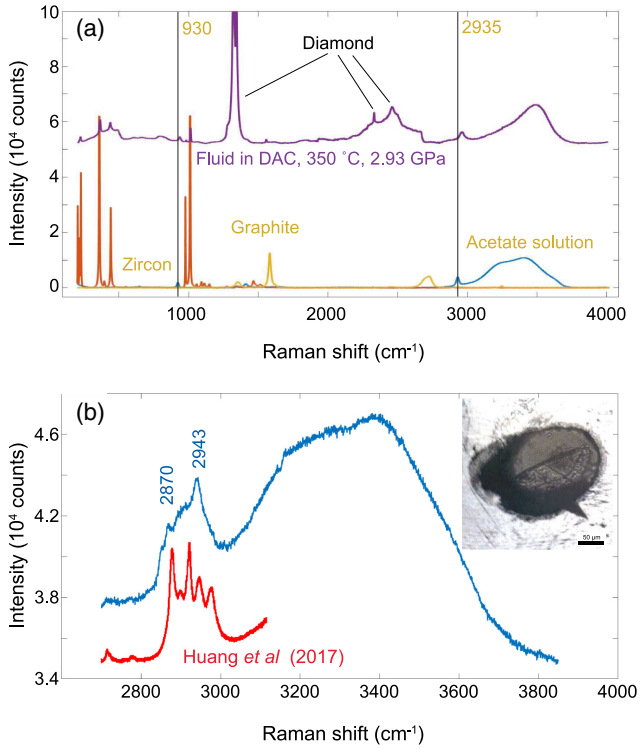

Figure 3 **(a)** *In situ* Raman spectrum of sodium acetate solution heated to 350 °C and 2.93 GPa inside an externally heated diamond cell. Reference spectra of the acetate solution at ambient conditions, of graphite and of zircon (used as pressure sensor in the cell) are also shown. The 930 cm^{-1} and 2935 cm^{-1} bands of the acetate are still seen in the solution, shifted to slightly higher wave numbers due to the elevated pressure. **(b)** Detail of the Raman spectrum of acetate solution after heating to 350 °C and 2.93 GPa and cooling to room temperature. New C–H stretching bands of hydrocarbons, likely isobutane and propane, can be observed. Data from Huang *et al.* (2017) obtained in a similar experiment are shown for comparison. The hydrocarbons form small droplets in the sample chamber (inset).

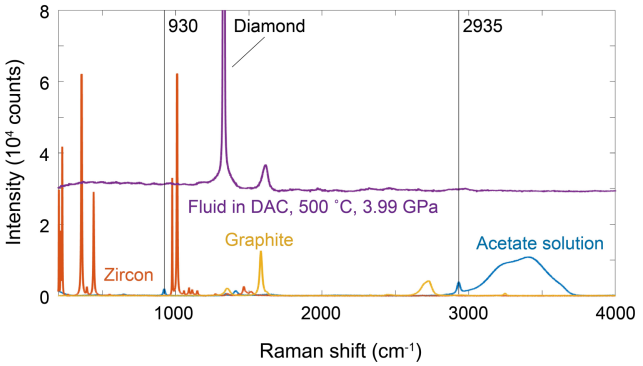

Figure 4 *In situ* Raman spectrum of sodium acetate solution heated to 500 °C and 3.99 GPa inside an externally heated diamond cell. Reference spectra of the acetate solution at ambient conditions, of graphite and of zircon (used as pressure sensor in the cell) are also shown. The 930 cm^{-1} and 2935 cm^{-1} bands of the acetate are not detectable anymore, while a graphitic material has formed by decomposition of the acetate.

with some hydrocarbons (containing C^{4-}) by partial disproportionation of the acetate (with an average carbon oxidation state of zero). Despite these results, which indicate partial decomposition, some acetate was still detectable in the solution. The charge from experiment AB3 was then rerun in experiment AB4, which reached 600 °C and 4.65 GPa, essentially the predicted stability field of acetate. However, already at 3.99 GPa and 500 °C, no acetate was detectable in the fluid anymore (Fig. 4). Instead, the Raman spectrum of a carbonaceous material resembling highly disordered graphite was detected. No acetate could be detected in the fluid after cooling it back to room temperature; instead, abundant dark, carbonaceous material was visible inside the cell (Fig. S-3), which yielded Raman spectra resembling highly disordered graphite.

Clear evidence for methane or CO_2 was not seen in any of the Raman spectra of the *in situ* experiments; however, traces may have remained undetected due to the proximity of the CH_4 stretching bands to those of the CH_3-group of acetate and of the CO_2 Fermi dyad to the main band of the diamond anvils.

Discussion

The results both from the piston cylinder and the *in situ* diamond cell experiments appear very consistent and suggest that, above 500 °C, acetate is not stable anymore in aqueous fluids and decomposes to a carbonaceous material. This observation has important consequences for the fate of subducted carbon. While carbon in oxidised form, *i.e.* as carbonates, may be readily mobilised during the release of aqueous fluids, the fate of reduced carbon during subduction is much less understood (Plank and Manning, 2019). Reduced carbon in the form of former organic material is abundant in many sediments. If acetate, which is highly water-soluble, were stable in aqueous fluids, such fluids would likely be very efficient in returning subducted carbon back to the surface. In the absence of such mobile organic species, graphitic material is likely almost insoluble in water and very poorly soluble in silicate melts (*e.g.*, Eguchi and Dasgupta, 2017), at least in an intermediate range of oxygen fugacities, where neither the oxidation to CO or CO_2 nor the reduction to CH_4 is thermodynamically favourable. Such graphitic material may therefore be recycled deep into the mantle during subduction. However, fluxing by external, particularly oxidised, fluids may be an efficient mechanism to dissolve reduced carbon and return it to the surface. Field evidence for the efficiency of such a process was presented by Vitale Brovarone *et al.* (2020). Moreover, at least at relatively shallow depth corresponding to pressures of 1 GPa, organic carbon may be significantly more fluid-soluble than well ordered graphite (Tumiati *et al.*, 2020).

The causes for the discrepancy between our experimental results and theoretical predictions (Sverjensky *et al.*, 2014, 2020) are uncertain. One possibility is that the causes are in the parametrisation of the Helgeson-Kirkham-Flowers model (Shock *et al.*, 1992). Here, the caloric and volumetric parameters for organic species may be poorly constrained. Uncertainties in some of the most basic properties of water at high pressure and high temperature may also limit the reliability of thermodynamic models. The predicted stability of ionic species in aqueous fluids very strongly depends on the precise value of the dielectric constant. However, up to now, direct experimental measurements of the dielectric constant have been limited to 550 °C and 0.5 GPa (Heger *et al.*, 1980). Moreover, while the stability of acetate as a main carbon species in deep subduction fluids appears rather unlikely in the light of the experimental results presented here, the stability of minor concentrations of organic species is still possible and requires further investigation. For example, oxalate $(COO)_2^{2-}$, the most simple dicarbonic acid ion, is known to form very strong complexes with many cations in aqueous solutions (*e.g.*, Krishnamurty and Harris, 1961).

Already minor concentrations of oxalate could therefore have a significant effect on the chemical transport properties of subduction zone fluids.

Acknowledgements

We thank Matthieu Galvez and an anonymous referee for constructive reviews which helped to improve the manuscript.

Editor: Horst R. Marschall

Additional Information

Supplementary Information accompanies this letter at http://doi.org/10.7185/geochemlet.2213.

Cite this letter as: Szlachta, V., Vlasov, K., Keppler, H. (2022) On the stability of acetate in subduction zone fluids. *Geochem. Persp. Let.* 21, 28–31. https://doi.org/10.7185/geochemlet.2213

References

Chou, I.M. (1986) Permeability of precious metals to hydrogen at 2 KB total pressure and elevated temperatures. *American Journal of Science* 286, 638–658. https://doi.org/10.2475/ajs.286.8.638

Eguchi, J. , Dasgupta, R. (2017) CO_2 content of andesitic melts at graphite-saturated upper mantle conditions with implications for redox state of oceanic basalt source regions and remobilization of reduced carbon from subducted eclogite. *Contributions to Mineralogy and Petrology* 172, 12. https://doi.org/10.1007/s00410-017-1330-8

Frezzotti, M.L. (2019) Diamond growth from organic compounds in hydrous fluids deep within the Earth. *Nature Communications* 10, 4952. https://doi.org/10.1038/s41467-019-12984-y

Heger, K., Uematsu, M., Franck, E.U. (1980) The static dielectric constant of water at high pressures and temperatures to 500 MPa and 550 °C. *Berichte der Bunsengesellschaft für Physikalische Chemie* 84, 758–762. https://doi.org/10.1002/bbpc.19800840814

Huang, F., Daniel, I., Cardon, H., Montagnac, G., Sverjensky, D.A. (2017) Immiscible hydrocarbon fluids in the deep carbon cycle. *Nature Communications* 8, 15798. https://doi.org/10.1038/ncomms15798.

Ito, K., Bernstein, H.J. (1956) The vibrational spectra of the formate, acetate, and oxalate ions. *Canadian Journal of Chemistry* 34, 170–178. https://doi.org/10.1139/v56-021

Krishnamurty, K.V., Harris, G.M. (1961) The chemistry of the metal oxalato complexes. *Chemical Reviews* 61, 213–246. https://doi.org/10.1021/cr60211a001

Li, Y. (2016) Immiscible C–H–O fluids formed at subduction zone conditions. *Geochemical Perspectives Letters* 3, 12–21. https://doi.org/10.7185/geochemlet.1702

Manning, C.E. (2004) The chemistry of subduction zone fluids. *Earth and Planetary Science Letters* 223, 1–16. https://doi.org/10.1016/j.epsl.2004.04.030

Manning, C.E., Frezzotti, M.L. (2020) Subduction-zone fluids. *Elements* 16, 395–400. https://doi.org/10.2138/gselements.16.6.395

Plank, T., Manning, C.E. (2019) Subducting carbon. *Nature* 574, 343–352. https://doi.org/10.1038/s41586-019-1643-z

Rüpke, L.H., Phipps Morgan, J., Hort, M., Connolly, J.A.D. (2004) Serpentine and the subduction zone water cycle. *Earth and Planetary Science Letters* 223, 17–34. https://doi.org/10.1016/j.epsl.2004.04.018

Rustioni, G., Audetat, A., Keppler, H. (2021) The composition of subduction zone fluids and the origin of the trace element enrichment in arc magmas. *Contributions to Mineralogy and Petrology* 176, 51. https://doi.org/10.1007/s00410-021-01810-8

Shock, E.L., Oelkers, E.H., Johnson, J.W., Sverjensky, D.A., Helgeson, H.C. (1992) Calculation of the thermodynamic properties of aqueous species at high pressures and temperatures. Effective electrostatic radii, dissociation constants and standard partial molal properties to 1000 °C and 5 kbar. *Journal of the Chemical Society, Faraday Transactions* 88, 803–826. https://doi.org/10.1039/FT9928800803

Sisson, T.W., Kelemen, P.B. (2018) Near-solidus melts of MORB + 4 wt% H_2O at 0.8–2.8 GPa applied to issues of subduction magmatism and continent formation. *Contributions to Mineralogy and Petrology* 173, 70. https://doi.org/10.1007/s00410-018-1494-x

Sverjensky, D.A., Huang, F. (2015) Diamond formation due to a pH drop during fluid–rock interactions. *Nature Communications* 6, 8702. https://doi.org/10.1038/ncomms9702

Sverjensky, D.A., Stagno, V., Huang, F. (2014) Important role for organic carbon in subduction-zone fluids in the deep carbon cycle. *Nature Geoscience* 7, 909–913. https://doi.org/10.1038/ngeo2291

Sverjensky, D., Daniel, I., Vitale Brovarone, A. (2020) The changing character of carbon in fluids with pressure. In: Manning, C.E., Lin, J.-F., Mao, W.L. (Eds.) *Carbon in Earth´s Interior. Geophysical Monograph 249*. American Geophysical Union, Washington, D.C., John Wiley and Sons, Inc., Hoboken, NJ, 259–269. https://doi.org/10.1002/9781119508229.ch22

Tatsumi, Y. (1989) Migration of fluid phases and genesis of basalt magmas in subduction zones. *Journal of Geophysical Research: Solid Earth* 94, 4697–4707. https://doi.org/10.1029/JB094iB04p04697

Tiraboschi, C., Tumiati, S., Sverjensky, D.A., Pettke, T., Ulmer, P., Poli, S. (2018) Experimental determination of magnesia and silica solubilities in graphite-saturated and redox-buffered high-pressure COH fluids in equilibrium with forsterite + enstatite and magnesite + enstatite. *Contributions to Mineralogy and Petrology* 173, 2. https://doi.org/10.1007/s00410-017-1427-0

Tumiati, S., Tiraboschi, C., Sverjensky, D.A., Pettke, T., Recchia, S., Ulmer, P., Miozzi, F., Poli, S. (2017) Silicate dissolution boosts the CO_2 concentrations in subduction fluids. *Nature Communications* 8, 616. https://doi.org/10.1038/s41467-017-00562-z

Tumiati, S., Tiraboschi, C., Miozzi, F., Vitale-Brovarone, A., Manning, C.E., Sverjensky, D.A., Milani, S., Poli, S. (2020) Dissolution susceptibility of glass-like carbon versus crystalline graphite in high-pressure aqueous fluids and implications for the behavior of organic matter in subduction zones. *Geochimica et Cosmochimica Acta* 273, 383–402. https://doi.org/10.1016/j.gca.2020.01.030

Vitale Brovarone, A., Tumiati, S., Piccoli, F., Ague, J.J., Connolly, J.A.D., Beyssac, O. (2020) Fluid-mediated selective dissolution of subducting carbonaceous material: Implications for carbon recycling and fluid fluxes at forearc depths. *Chemical Geology* 549, 119682. https://doi.org/10.1016/j.chemgeo.2020.119682

Geochemical Perspectives Letters

On the stability of acetate in subduction zone fluids

V. Szlachta, K. Vlasov, H. Keppler

Supplementary Information

The Supplementary Information includes:

- Experimental Methods
- Figures S-1 to S-4
- Supplementary Information References

Experimental Methods

Piston cylinder experiments

Piston cylinder experiments (Boyd and England, 1960) were carried out using mechanically sealed silver capsules with a length of 10 mm, an outer diameter of 5 mm and a wall thickness of 1 mm. A solution of 10 wt. % $CH_3COONa \cdot 3 H_2O$ (Merck, 99.5 %) in distilled water was loaded into the capsules together with SiO_2 powder (Chempur, 99.9%) for mechanical stabilisation. The fluid/solid ratio ranged from 0.34 to 0.9. Experiments were carried out with low-friction ½ inch NaCl-MgO assemblies containing a stepped graphite heater in an automated, end-loaded piston cylinder press (Voggenreiter GmbH, Mainleus, Germany). This device contains two spindle presses that allow a precise control of the oil pressures on the master ram and the endload, such that continuous compression and decompression profiles can be run under computer-control. Experiments were slowly pressurised and de-pressurised over 19–21 hours in order to limit bomb and piston failures at 5 GPa. Runs were heated to the target temperature of 600 °C within 30 minutes and cooled down at the end of the run again within about 30 minutes. However, the "zero time" experiment was heated more rapidly within ~10 min, maintained for ~8 min at 600 °C and cooled to room temperature in 9 minutes. Temperatures were measured by a type S (Pt-PtRh) thermocouple close to the sample and controlled by a Eurotherm controller. A constant friction correction of −0.12 GPa was applied to the nominal pressures. This correction was calibrated by the quartz–coesite transition near 3 GPa and by the density of synthetic fluid inclusions at 800 °C and 0.5–1.0 GPa.

Diamond anvil cell experiments

In situ spectroscopic experiments were carried out with a Bassett-type externally heated diamond anvil cell (Bassett *et al*., 1993) using synthetic, low-fluorescence type II-a diamond anvils with 700 µm culet. The cell was heated using molybdenum wires around the tungsten carbide seats supporting the diamonds. Temperature was monitored using K-type thermocouples (NiCr-Ni) directly attached to the diamonds. Gaskets made of Re or Ir with an initial thickness of 250 µm and a 150–180 µm drillhole were used. The 10 wt. % sodium acetate solution was loaded into the sample chamber together with a small zircon crystal (natural zircon from Sri Lanka) as a pressure sensor. The cell was flushed during experiments with a 98 % Ar–2 % H_2 gas mixture to prevent oxidation of the molybdenum heaters and the diamonds. Pressures during runs were determined based on the Raman shift of the $\nu_3(SiO_4)$ band in zircon (~1008 cm^{-1}) following the calibration of Schmidt *et al*. (2013). The objectives of the Raman spectrometer were cooled with air at high temperatures.

Raman spectroscopy

Raman spectra were measured using a Horiba/Jobin Yvon LabRam HR UV confocal Raman spectrometer in backscatter geometry. The 514 nm line of an argon laser with 75–200 mW output power was used for excitation. Spectra were measured with a 50× objective, a 1800 groves/mm grating and a Peltier-cooled CCD detector. The confocal pinhole was set to 100–1000 µm, the spectral resolution was about 3.5 cm^{-1}, and each spectrum was typically collected using two 35 s accumulations.

Supplementary Figures

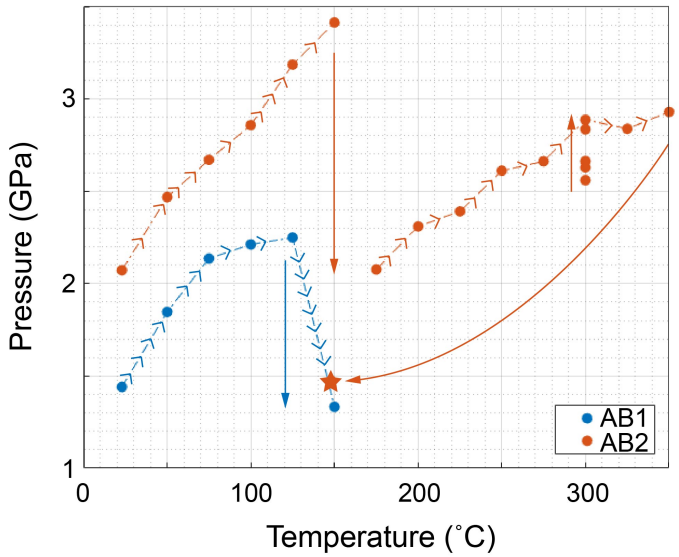

Figure S-1 Pressure-temperature paths of the diamond anvil cell runs AB1 and AB2. The star at 148 ° C for run AB2 indicates the end of run when the gasket cracked. Straight arrows indicate pressure addition (by tightening the cell) or pressure drop (due to gasket flow or leakage).

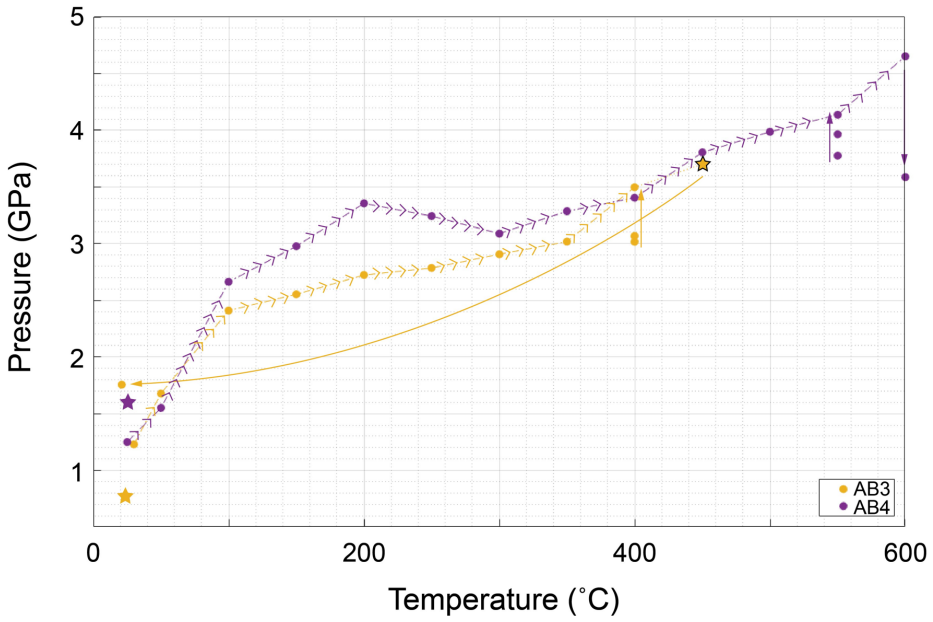

Figure S-2 Pressure-temperature paths of the diamond anvil cell runs AB3 and AB4. The black-outlined star for run AB3 at 450 °C marks a heater failure. The data point at 21 °C for run AB3 indicates the residual pressure immediately after the run. Stars indicates the pressures measured on the day after the runs.

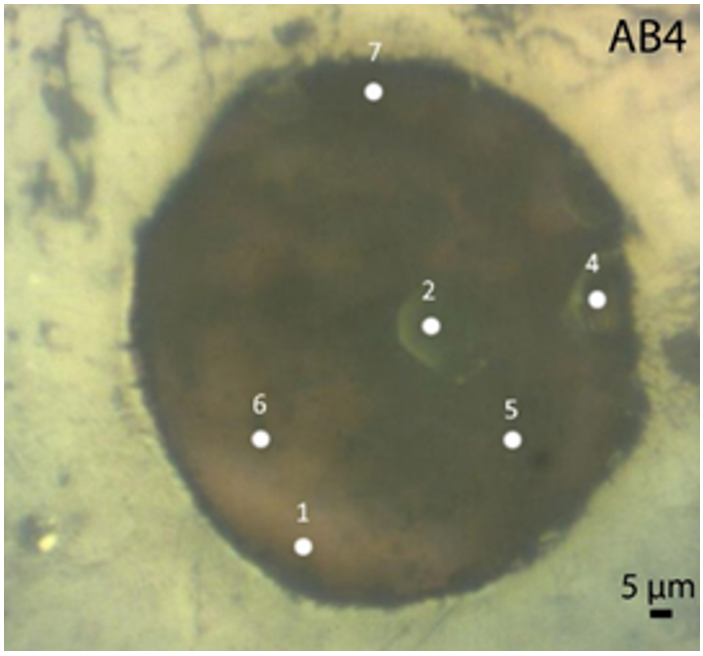

Figure S-3 Sample chamber of experiment AB4 after cooling back to room temperature from 600 °C and 4.65 GPa. Note the dark, carbonaceous material floating inside the solution. White spots refer to the location of Raman measurements given in Figure S-4.

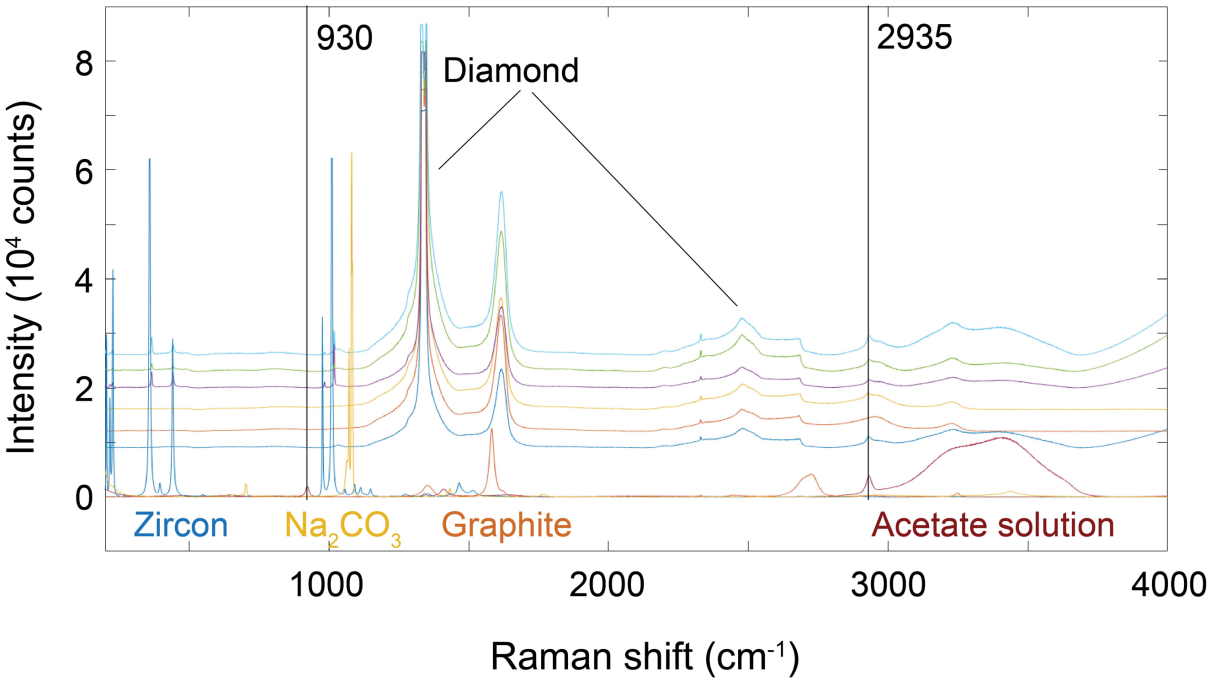

Figure S-4 Raman spectra of quench products from run AB4. The presence of a carbonaceous material resembling disordered graphite is obvious in all spectra. While there is a band in the C-H stretching region close to 2935 cm^{-1}, similar to acetate, the C-C stretching band of acetate at 930 cm^{-1} is clearly missing. The sequence of the spectra from bottom to top is from point 1 to point 7 according to Figure S-3.

Supplementary Information References

Bassett, W.A., Shen, A.H., Bucknum, M., Chou, I.M. (1993) A new diamond anvil cell for hydrothermal studies to 2.5 GPa and from −190 to 1200 °C. *Review of Scientific Instruments* 64, 2340–2345. https://doi.org/10.1063/1.1143931

Boyd, F.R., England, J.L. (1960) Apparatus for phase-equilibrium measurements at pressures up to 50 kbars and temperatures up to 1750°C. *Journal of Geophysical Research* 65, 741–748. https://doi.org/10.1029/JZ065i002p00741

Schmidt, C., Steele-MacInnis, M., Watenphul, A., Wilke, M. (2013) Calibration of zircon as a Raman spectroscopic pressure sensor to high temperatures and application to water-silicate melt systems. *American Mineralogist* 98, 643–650. https://doi.org/10.2138/am.2013.4143